Received: 15 January 2018 | Revised: 4 April 2018 | Accepted: 17 April 2018

DOI: 10.1002/pip.3021

RESEARCH ARTICLE

WILEY PROGRESS IN PHOTOVOLTAICS

Theoretical model and simulation of carrier heating with effects of nonequilibrium hot phonons in semiconductor photovoltaic devices

Chin-Yi Tsai

Department of Applied Physics, National University of Kaohsiung, 700 Kaohsiung University Rd, Nanzih District, Kaohsiung 811, Taiwan

Correspondence
Chin-Yi Tsai, Department of Applied Physics, National University of Kaohsiung, 700 Kaohsiung University Rd, Nanzih District, Kaohsiung 811, Taiwan.
Email: chinyitsai@hotmail.com; cytsai@nuk.edu.tw

Abstract

A theoretical model and its rate equations of carrier number and energy densities are proposed and presented for calculating carrier heating in semiconductor photovoltaic devices. The rate equation for carrier number density is the Shockley-Queisser theoretical model, while the rate equation for carrier energy density includes the carrier interband energy relaxation via radiative recombination and the intraband energy relaxation via the interactions between carriers and polar longitudinal optical phonons. The carrier intraband energy relaxation is calculated by incorporating the effects of nonequilibrium hot phonons and the Thomas-Fermi static screening. This model and its rate equations are employed for numerical simulations of the magnitude of carrier heating and its effects on the current-voltage relations of bulk GaAs solar cells under different concentration ratios and with different widths of the active region. The simulation results demonstrate that carrier temperature in general heats up to 400 to 900 K at short-circuit operating condition. This carrier heating cools down to lattice temperature when the device approaches its open-circuit point. Based on these numerical results, effects of carrier heating on the performance of conventional solar cells and also their implications for the design of hot-carrier solar cells will be discussed.

KEYWORDS

carrier energy relaxation, carrier heating, hot carriers, hot phonons, photovoltaic, simulation, solar cell, theory

1 | INTRODUCTION

Hot carriers in semiconductor devices are not only an interesting and important subject but they also have tremendous technical impacts on the devices' performances and applications,[1,2] especially for solar cells (or photovoltaic devices). Recently, several interesting results regarding the issue of hot carriers in solar cells have been demonstrated and discussed.[3-6] In addition, ongoing efforts have been focused on the theoretical aspects of designing and realizing hot-carrier solar cells, in which the kinetic energy of hot carriers can be extracted as an additional output power and could therefore dramatically enhance the efficiency from conventional devices.[7-15] However, to exploit the possibility of converting the kinetic energy of hot carriers into useful electrical power output, it is inevitably necessary to know the magnitude of carrier heating inside a device. In other words, for the purpose of studying the effects of hot carriers on devices and also their possible applications, it is essential to experimentally determine or theoretically evaluate and estimate the carrier temperature inside working devices.

To facilitate the discussion on the topic of hot carriers in solar cells, 4 different temperature systems can be categorized into consideration: the Sun, the carriers, the solar cell (the device), and the ambient environment, as schematically shown in Figure 1. The solar AM0 (air mass zero) spectral irradiance can be well fitted by a black body

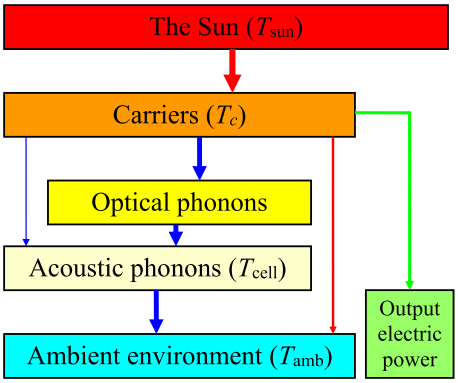

FIGURE 1 Schematic diagram shows the 4 different temperature systems in an operating solar cell: The sun, the carriers, the solar cell (the device), and the ambient environment. The arrows indicate the energy flow among them. The colors of the arrows indicate the processes of phonons (in blue), photons (in red), and carriers (in green) [Colour figure can be viewed at wileyonlinelibrary.com]

radiation with a temperature roughly about 5800 K, as shown in Figure 2, which can then be designated as the surface temperature of the Sun's photosphere, ie, $T_{sun} \approx 5800$ K. In a semiconductor solar cell (or in general, semiconductor device), the carries comprised by electrons in the conduction band and holes in the valence band can be characterized by a carrier temperature T_c, while the thermal vibrations of ions, atoms, and molecules (ie, phonons) of the host material are characterized by a cell temperature T_{cell} (or more precisely called as lattice temperature). If carrier temperature T_c is significantly different from its cell temperature T_{cell}, then the device operates with the presence of hot carriers. The temperature of the surrounding environment of a solar cell can be roughly characterized as the ambient temperature. The ambient temperature is usually set to the room temperature as T_{amb} = 25 °C = 298.15 K to agree with the standard test condition (STC) for solar cells and modules.

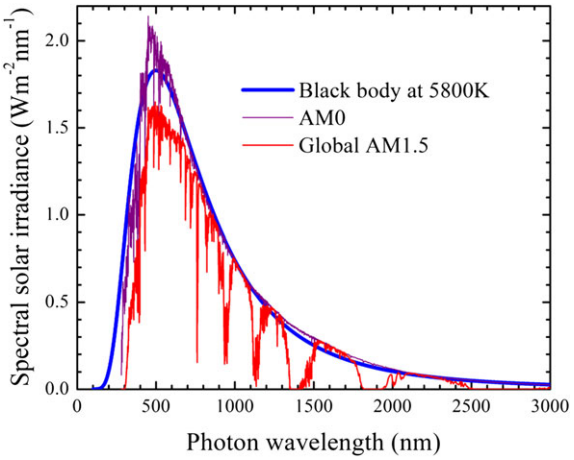

FIGURE 2 Spectral solar irradiance of the air mass zero (AM0), the global AM1.5, and the black-body radiation with temperature of 5800 K. The AM0 and AM1.5 data points are the standard solar spectral irradiance data ASTM-173-03 [Colour figure can be viewed at wileyonlinelibrary.com]

In fact, the condition of $T_{sun} > T_c > T_{cell} > T_{amb}$ exists for a working solar cell. However, if the difference between T_c and T_{cell} are assumed to be minute and insignificant, then the effects of hot carriers can thus be approximately neglected. Such an assumption is commonly adopted by conventional theories for solar cells. In other words, the condition $T_{sun} > T_c = T_{cell} > T_{amb}$ is conjecturally presumed for most theories of solar cells. Attention and interest are usually focused on the subjects regarding their temperature coefficients. In a working solar cell, its cell temperature is certainly higher than the ambient temperature (ie, $T_{cell} > T_{amb}$) and the increase of the cell temperature will normally deteriorate the output power of the device. This effect can be empirically yet conveniently characterized by a temperature coefficient C_T. If the output power of a solar cell (or module) is a function of temperature, $W_{out}(T)$, then the temperature coefficient is defined as[16]

$$C_T = \frac{[W_{out}(T_{cell}) - W_{out}(T_{amb})]/W_{out}(T_{amb})}{T_{cell} - T_{amb}}. \quad (1)$$

Nonetheless, to focus on the effects of hot carrier, the issue regarding the temperature coefficient and the thermal behavior associated with the cell temperature will not be discussed in this work. In fact, the overall device heating phenomenon is a very complicated issue in which carrier heat transport and lattice thermal conduction (ie, phonon heat transport) need to be considered simultaneously. Such an issue is of course beyond the scope and capacity of this study. As a result, the cell temperature will be expediently set to be equal to the ambient temperature in this study. In other words, the condition of $T_{sun} > T_c > T_{cell} = T_{amb}$ will therefore be expediently assumed throughout this work.

Of course, it is very desirable to theoretically calculate the magnitude of carrier heating in a device and to study their effects on the device's performance if experimental results are inaccessible. However, theoretical calculations or simulations on the variation of carrier temperatures within an operating solar cell are in fact not a straightforward task, especially when involving the carrier intraband energy relaxation processes via carrier-phonon interactions. Conventionally, carrier intraband energy relaxation processes are summarily discussed by assigning a time constant, the carrier energy relaxation time. However, if its chosen value is too large, then the magnitude of carrier heating will be overestimated. Contrarily, if it is too small, then it will be underestimated. As will be shown in this work, carrier energy relaxation time or rate is strongly dependent on the carrier density and temperature. Hence, it is rather inappropriate to treat carrier energy relaxation time as a constant value in studying carrier heating problems.

More advanced techniques, such as the ab initio method[17] and Monte Carlo method and simulation,[18-20] can be employed to study the carrier heating problems. However, simulations using these methods for semiconductor devices are usually too involved and laborious to produce the results for a specific problem, for example, in the case of intraband carrier energy relaxation involving effects of nonequilibrium hot phonons. The issue regarding hot-phonon effects will be elaborately discussed in detail in the following. Our results evidently demonstrate the necessity of incorporating effects of nonequilibrium hot phonons in studying carrier energy relaxation processes.

In this work, to effectively study carrier heating problems in photovoltaic devices, a simple yet realistic theoretical model will be proposed and presented for calculating carrier heating with effects of nonequilibrium hot phonon. Rate equations of carrier number and energy densities will be given. Numerical results will be given to GaAs material due to its well documented physical parameters, such as the lifetime of longitudinal optical (LO) phonons. The degree of carrier heating and the variations of carrier temperature of an operating solar cell will be numerically simulated and calculated.

The contents of this work are organized as follows: In Section 2, the theoretical model will be outlined and explained. Rate equations of carrier number and energy densities will be given and discussed in Section 2.1. The calculation of radiative recombination will be given in Section 2.2. The calculation of the intraband carrier energy relaxation will be given and explained in Section 2.3. The incorporation of the nonequilibrium hot phonons into the intraband carrier energy relaxation will be presented in Section 2.4. Simulations of the carrier heating problems and their effects on the current-voltage (*J*-*V*) relation of solar cells will be discussed in Section 3. The conclusion of this study will be addressed in Section 4.

2 | THEORETICAL MODEL

To calculate carrier heating with effects of nonequilibrium hot phonons in photovoltaic devices, a theoretical model and its rate equations will be proposed and explained in this work. These rate equations result from the balance equations for carrier number and energy. This model will focus on the carrier generation-recombination processes in the active region by deliberately neglecting the problems of carrier transport of population and energy. In other words, it will completely omit the roles of carrier drift and diffusion currents and also the carrier heat current. Nevertheless, this model can still incorporate carrier transport problems by introducing additional transport times to characterize their effects as in the previous discussion,[21] but this only complicates the essential role of hot carriers and hot phonons. In short, this model provides a simple but convenient way to estimate the magnitude of carrier heating and to assess their effects on devices' performance.

2.1 | Rate equations

Rate equations for carrier number and energy densities in semiconductor photovoltaic devices are given as follows:

$$\frac{dn}{dt} = \frac{1}{qL}(J_{\text{gen}} - J_{\text{rec}} - J), \tag{2}$$

$$\frac{du}{dt} = \frac{1}{L}(p_{\text{gen}} - p_{\text{rec}} - J{\cdot}V) + \left(\frac{du}{dt}\right)_{\text{intra}}. \tag{3}$$

Here, n and u denote the carrier number and energy densities, respectively. In this work, the Fermi-Dirac distribution function will be employed to numerically calculate the carrier number and energy densities. q is the elementary charge. J represents the output current density from photovoltaic devices. J_{gen} and J_{rec} are the current densities resulting from the carrier generation and recombination processes, respectively. Their associated power density fluxes are represented by p_{gen} and p_{rec}, respectively. L is the width of the active region where the photovoltaic action applies and it is given as a device parameter in this model. V is the output voltage from photovoltaic devices and is assumed to be equal to the electrochemical potential (ie, quasi-Fermi level) difference between electron and holes. The carrier interband energy relaxation to photons (as in radiative recombination processes) and phonons (as in the Shockley-Read-Hall [SRH] recombination) is given by the p_{rec} term, while the carrier intraband energy relaxation rate mainly via phonon emission is given by the $(du/dt)_{\text{intra}}$ term. It should be noted that, without Equation (3), Equation (2) alone is in fact identical to the Shockley-Queisser (SQ) theoretical model proposed for solar cells.[22]

2.2 | Radiative recombination

The SRH, Auger, and radiative processes are 3 carrier recombination processes in semiconductor devices; therefore,

$$J_{\text{rec}} = J_{\text{SRH}} + J_{\text{rad}} + J_{\text{Aug}}. \tag{4}$$

Auger recombination proceeds within carriers themselves and do not relax energy to photons or phonons (except for semiconductors with indirect band gap where phonons will participate in the Auger processes). Its roles in carrier energy relaxation can therefore be presumably ignored. The SRH processes mostly result from defect-assisted phonon emission and thus only contribute to the interband carrier energy relaxation processes. Because the SRH processes are defect-related, their contributions in interband carrier energy relaxation can range widely from being primarily significant for defect-rich materials to almost negligible for nearly defect-free materials. In other words, for direct-band-gap semiconductors or nearly defect-free materials, the magnitude of SRH recombination in the carrier interband energy relaxation is usually much smaller than radiative recombination. As a result, this work will only focus on radiative recombination while Auger and SRH recombination will be deliberately omitted for simplicity. Therefore, $J_{\text{rec}} = J_{\text{rad}}$ will be assumed in the following discussion.

In radiative recombination, current densities due to the carrier generation and recombination can be calculated from

$$J_{\text{gen}} = q\int_0^\infty a(E)\phi_{\text{in}}(E)dE, \tag{5}$$

$$J_{\text{rad}} = q\int_0^\infty e(E)\phi_{\text{out}}(E)dE. \tag{6}$$

Here $\phi_{\text{in}}(E)$ in Equation (5) denotes the input spectral flux of photon number density absorbed by carriers where E is the photon energy. This absorption process is characterized by the absorption quantum efficiency $a(E)$. Similarly, $\phi_{\text{out}}(E)$ in Equation (6) represents the output spectral flux of photon number density emitted by carriers. This emission process is characterized by the emission quantum efficiency $e(E)$. From Equations (5) and (6), energy density fluxes (ie, power intensity) associated with the correspondent carrier generation and

recombination are given as

$$p_{gen} = \int_0^\infty a(E) E \phi_{in}(E) dE, \tag{7}$$

$$p_{rad} = \int_0^\infty e(E) E \phi_{out}(E) dE. \tag{8}$$

The input lights come from 2 sources for solar cells: the incident sunlight and the radiation from the ambient environment:

$$\phi_{in}(E) = \phi_{sun}(E) + \phi_{amb}(E). \tag{9}$$

The input sunlight is chosen to be the global AM1.5 standard solar irradiance (ASTM-173-03) to agree with the STC. As a result, the spectral flux of photon number density from the incident sunlight $\phi_{sun}(E)$ is set as (as shown in Figure 3)

$$\phi_{sun}(E) = \phi_{ASTM}(E). \tag{10}$$

The spectral flux of photon number density from the radiation of the ambient environment is usually assumed to be a black-body radiation that can be calculated as (see Appendix A)

$$\phi_{amb}(E) = \frac{2\pi E^2}{h^3 c^2} \frac{1}{e^{E/k_B T_{amb}} - 1}, \tag{11}$$

in which T_{amb} = 25 °C = 298.15 K at the STC of solar cells and modules.

In Equations (5) and (7), $a(E)$ is the quantum efficiency of light absorption which characterizes the ratio between the number of carriers generated by the absorption of photons to the number of the incident photons. In this work, the ideal quantum efficiency will be assumed as

$$a(E) = H(E - E_g), \tag{12}$$

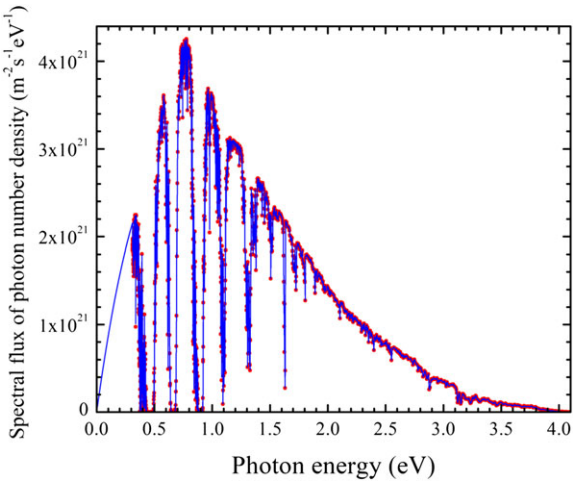

FIGURE 3 Spectral photon number density flux of standard global air mass 1.5 solar spectral irradiance data ASTM-173-03. The red dots are the original data points, and the blue line is the result from interpolation. Note that the data below 0.3 eV are modeled by a black-body radiation with temperature of 5800 K and 10% attenuation through Earth's atmosphere [Colour figure can be viewed at wileyonlinelibrary.com]

where $H(x)$ is the Heaviside step function and E_g is the band gap energy of semiconductors. By the argument of the principle of detailed balance, the emission quantum efficiency $e(E)$ can be assumed the same with the absorption one $a(E)$:

$$e(E) = a(E). \tag{13}$$

Without the consideration of hot carrier effects; ie, $T_c = T_{amb} = T$, the output radiation flux is shown to be related the ambient radiation as

$$\phi_{out}(E) = \phi_{amb}(E) \exp\left(\frac{qV}{k_B T}\right), \tag{14}$$

Here, qV is defined as

$$qV \equiv E_{Fc} - E_{Fv}, \tag{15}$$

where E_{Fc} and E_{Fv} denote the electrochemical potential energies (ie, the quasi-Fermi levels) of electrons in the conduction band and holes in the valence band, respectively. In a photovoltaic device, the output voltage V basically results from the difference in the electrochemical potentials between electrons and holes at 2 opposite ends of the device if other voltage-drop effects, such as series resistance, are neglected.

If Equation (14) is implemented, the J-V relation resulting from carrier radiative generation/recombination processes will become an exponential form similar to an ideal diode as

$$J = J_{gen} - J_{rec} = J_{sun} - (J_{rec} - J_{amb}) = J_{sun} - J_0\left(e^{V/V_T} - 1\right) = J_{sun} - J_{dark}, \tag{16}$$

where the thermal voltage V_T is defined as $V_T = k_B T/q$. Equation (16) simply demonstrates that the output current from a photovoltaic device is in fact a superposition of the photocurrent and the dark current. Here, the reverse saturation current density J_0 in Equation (16) is defined as

$$J_0 = J_{amb} = q\int_{E_g}^\infty \phi_{amb}(E) dE. \tag{17}$$

Note that when the device works without the incident sunlight; ie, $\phi_{sun} = 0$ and $V \neq 0$, $J = -J_{dark}$, the dark current will become

$$J_{dark} = q\int_{E_g}^\infty \phi_{out}(E) dE - q\int_{E_g}^\infty \phi_{amb}(E) dE = J_0\left(e^{qV/k_B T} - 1\right), \tag{18}$$

which bears the exact same form as the J-V relation of an ideal diode.

This diode-like J-V relation purely results from the carrier generation-recombination processes. In the short-circuit condition of $V = 0$ in Equation (16), the short circuit current density J_{sc} is exactly equal to the photocurrent density from the solar irradiance,

$$J_{sc} = J_{sun} = q\int_{E_g}^\infty \phi_{sun}(E) dE. \tag{19}$$

On the other hand, in the open-circuit condition of $J_{out} = 0$ in Equation (16), the open-circuit voltage becomes

$$V_{oc} = V_T \ln\left(\frac{J_{sc}}{J_0}+1\right) = V_T \ln\left[\frac{\int_{E_g}^{\infty}\phi_{sun}(E)dE}{\int_{E_g}^{\infty}\phi_{amb}(E)dE}+1\right], \tag{20}$$

Equations (19) and (20) are the explicit formulas for calculating the short-circuit current density and the open-circuit voltage, respectively.

The input optical power from the incident sunlight on a solar cell is

$$P_{in} = A\int_{E_g}^{\infty} E\phi_{sun}(E)dE, \tag{21}$$

where A is the effective irradiated area of the device. The output electrical power generated from a solar cell is

$$P_{out} = I_{out}V_{out} = A\cdot J\cdot V. \tag{22}$$

Note that here $I_{out} = A \cdot J$ is assumed which means that the device has 100% carrier collection efficiency in the SQ model. Consequently, the conversion efficiency of a solar cell is defined as the ratio between the maximum output electrical power P_{out}^{max} and the input optical power:

$$\eta = \frac{P_{out}^{max}}{P_{in}} = \frac{J_{max}\cdot V_{max}}{P_{in}/A} = \frac{J_{sc}\cdot V_{oc}\cdot FF}{P_{in}/A}. \tag{23}$$

where J_{max} and V_{max} denote the output current density and voltage at the maximum output power point, respectively. FF denotes as the fill factor.

In short, without the consideration of hot-carrier effects, ie, the carrier temperature equals the ambient temperature, the theoretical model presented by Equation (2) will simply yield a J-V relation of an ideal diode the same as the SQ model.[22] On the contrary, with the hot-carrier effects from incorporating Equation (3), the carrier temperature will no longer be equal to the ambient temperature, ie, $T_c \neq T_{amb}$. Under such circumstances, the photon density flux emitted by carriers is given by

$$\phi_{out}(E) = \phi_{amb}(E)\exp\left(\frac{\eta_C E}{k_B T_{amb}}\right)\exp\left[\frac{(1-\eta_C)qV}{k_B T_{amb}}\right] \tag{24}$$

where η_C is named as the Carnot's efficiency and defined by

$$\eta_C \equiv 1-\frac{T_{amb}}{T_c}. \tag{25}$$

Equations (24) and (25) can be derived from the principle of detailed balance as presented and discussed in Appendix B. Apparently, if $T_c = T_{amb}$ and thus $\eta_C = 0$, Equation (24) will be the same as Equation (14). Consequently, with the effects of hot carriers, the output current density will become

$$\begin{aligned} J &= J_{sun} + J_{amb} - J_{rad} \\ &= q\int_{E_g}^{\infty}\phi_{sun}(E)dE + q\int_{E_g}^{\infty}\phi_{amb}(E)dE \\ &\quad - \exp\left[\frac{(1-\eta_C)qV}{k_B T_{amb}}\right] q\int_{E_g}^{\infty}\phi_{amb}(E)\exp\left(\frac{\eta_C E}{k_B T_{amb}}\right)dE. \end{aligned} \tag{26}$$

Apparently, with the effects of hot carriers, the J-V relation is no longer a simple exponential form as an ideal diode. In the short-circuit condition of $V = 0$, Equation (26) becomes

$$J_{sc} = q\int_{E_g}^{\infty}\phi_{sun}(E)dE - q\int_{E_g}^{\infty}\phi_{amb}(E)\left[\exp\left(\frac{\eta_C E}{k_B T_{amb}}\right)-1\right]dE. \tag{27}$$

Again, if $T_c = T_{amb}$ and thus $\eta_C = 0$, Equation (27) will be the same as Equation (19). The short-circuit current density calculated by Equation (27) with hot-carrier effects is no longer solely contributed from the incident sunlight as in the case without hot-carrier effects in Equation (19). The enhanced radiative recombination from hot carriers will reduce the short-circuit current density as the results predicted from Equation (27). On the other hand, in the open-circuit condition of $J = 0$, unlike the cases without the hot-carrier effects of Equation (20), there is no explicit expression for calculating the open-circuit voltage for the cases with the hot-carrier effects. It can only be calculated numerically.

2.3 | Intraband carrier energy relaxation

The carrier energy density can be calculated by summing the carrier energy $E_{\mathbf{k}}$ associated with statistically average carrier number $f_{\mathbf{k}}$ at each $\mathbf{k}$-state as

$$u = \frac{2}{V_c}\sum_{\mathbf{k}} E_{\mathbf{k}} f_{\mathbf{k}}, \tag{28}$$

where V_c is the volume of carriers and the factor of 2 accounts for the degeneracy of 2 spins associated with each $\mathbf{k}$-state. Assuming that carriers have sufficient carrier-carrier scatterings to maintain their quasi-equilibrium condition with a common chemical potential energy μ and temperature T_c, $f_{\mathbf{k}}$ observes the Fermi-Dirac distribution as

$$f_{\mathbf{k}} = \left[\exp\left(\frac{E_{\mathbf{k}}-\mu}{k_B T_c}\right)+1\right]^{-1}, \tag{29}$$

where $E_{\mathbf{k}}$ denotes carrier kinetic energy, μ is the chemical potential, and T_c is the carrier temperature. According to Equation (29), the change of carrier population (characterized by the chemical potential) or the carrier temperature will certainly change the $f_{\mathbf{k}}$ and thus the total carrier kinetic energy as

$$\left(\frac{du}{dt}\right)_{intra} = \frac{2}{V_c}\sum_{\mathbf{k}} E_{\mathbf{k}}\left(\frac{df_{\mathbf{k}}}{dt}\right)_{intra}. \tag{30}$$

The intraband energy relaxation mainly proceeds by carrier-phonon interactions; the change rate of the $f_{\mathbf{k}}$ can be contributed by all 4 possible processes as

$$\begin{aligned} \left(\frac{df_{\mathbf{k}}}{dt}\right)_{intra} = \frac{2\pi}{\hbar}\sum_{\mathbf{q}}|M_{\mathbf{q}}|^2\Big[&(N_{\mathbf{q}}+1)f_{\mathbf{k}+\mathbf{q}}(1-f_{\mathbf{k}})I^2(\mathbf{k},\mathbf{k}+\mathbf{q})\delta(E_{\mathbf{k}}-E_{\mathbf{k}+\mathbf{q}}+\hbar\omega_{\mathbf{q}}) \\ &+N_{\mathbf{q}}f_{\mathbf{k}-\mathbf{q}}(1-f_{\mathbf{k}})I^2(\mathbf{k},\mathbf{k}-\mathbf{q})\delta(E_{\mathbf{k}}-E_{\mathbf{k}-\mathbf{q}}-\hbar\omega_{\mathbf{q}}) \\ &-N_{\mathbf{q}}f_{\mathbf{k}}(1-f_{\mathbf{k}+\mathbf{q}})I^2(\mathbf{k},\mathbf{k}+\mathbf{q})\delta(E_{\mathbf{k}}-E_{\mathbf{k}+\mathbf{q}}+\hbar\omega_{\mathbf{q}}) \\ &-(N_{\mathbf{q}}+1)f_{\mathbf{k}}(1-f_{\mathbf{k}-\mathbf{q}})I^2(\mathbf{k},\mathbf{k}-\mathbf{q})\delta(E_{\mathbf{k}}-E_{\mathbf{k}-\mathbf{q}}-\hbar\omega_{\mathbf{q}})\Big] \end{aligned} \tag{31}$$

where $N_{\mathbf{q}}$ denotes the statistically average phonon number at wave vector $\mathbf{q}$, $|M_{\mathbf{q}}|$ is the carrier-phonon interaction matrices, and $I(\mathbf{k}, \mathbf{k} \pm \mathbf{q})$ is the integral 2 carriers' Bloch functions at 2 different wave vectors. $I(\mathbf{k}, \mathbf{k} \pm \mathbf{q}) \approx 1$ is usually assumed for intraband transitions of electrons in the conduction band. $\delta(E_{\mathbf{k}} - E_{\mathbf{k} \pm \mathbf{q}} \pm \hbar\omega_{\mathbf{q}})$ is the Dirac delta

function in which the conservation of energy is complied. However, it is not straightforward to incorporate the effects of nonequilibrium hot phonons into Equation (31). Alternatively, this problem can be solved by employing another equivalent method by calculating the net mission rate of phonons as

$$\left(\frac{dN_{\mathbf{q}}}{dt}\right)_{\text{intra}} = \frac{2\pi}{\hbar}\sum_{\mathbf{k}}|M_{\mathbf{q}}|^2 I^2(\mathbf{k},\mathbf{k}-\mathbf{q}) \left[+(N_{\mathbf{q}}+1)f_{\mathbf{k}}(1-f_{\mathbf{k}-\mathbf{q}})\delta(E_{\mathbf{k}}-E_{\mathbf{k}-\mathbf{q}}-\hbar\omega_{\mathbf{q}}) - N_{\mathbf{q}}f_{\mathbf{k}-\mathbf{q}}(1-f_{\mathbf{k}})\delta(E_{\mathbf{k}}-E_{\mathbf{k}-\mathbf{q}}-\hbar\omega_{\mathbf{q}})\right]. \quad (32)$$

The first term in Equation (32) represents a carrier at a **k** state emitting a phonon with energy $\hbar\omega_{\mathbf{q}}$ and wave vector **q** and transiting into a **k** − **q** state. The second term represents a carrier at a **k** state absorbing a phonon and transiting into a **k** − **q** state. Then, the intraband carrier energy relaxation rate can be calculated by the summation of all the phonon energy emitted by carriers as

$$\left(\frac{du}{dt}\right)_{\text{intra}} = -\frac{1}{V_c}\sum_{\mathbf{q}}\hbar\omega_{\mathbf{q}}\left(\frac{dN_{\mathbf{q}}}{dt}\right)_{\text{intra}}. \quad (33)$$

In general, carriers can interact with 4 types of phonons: polar optical phonons, deformation potential optical phonons, deformation potential acoustic phonons, and piezoelectric acoustic phonons.[23] Their interaction matrices are listed in the following:

$$\begin{aligned}|M_q|^2 &= \frac{e^2\hbar\omega_{\text{LO}}}{2\varepsilon_0 q^2 V_n}\left(\frac{1}{K_\infty}-\frac{1}{K_s}\right) && \text{polar optical phonon}\\ &= \frac{D_O^2\hbar^2}{2\rho_L\hbar\omega_O V_n} && \text{deformation potential optical phonon}\\ &= \frac{\Xi^2\hbar^2 q^2}{2\rho_L\hbar\omega_q V_n} && \text{deformation potential acoustic phonon}\\ &= \frac{e^2\bar{e}_{av}^2\hbar^2}{2\varepsilon_s^2\rho_L\hbar\omega_q V_n} && \text{piezoelectric acoustic phonon}\end{aligned} \quad (34)$$

Here, ε_0 is the vacuum permittivity. $\hbar\omega_{\text{LO}}$ is the LO phonon energy. V_n is the volume of phonons. The volumes for carriers and phonon are generally assumed to be equal for the case of bulk semiconductors; ie, $V_c = V_n$. $K_\infty(K_s)$ is the high-frequency (static) dielectric constant. D_O is the deformation potential of optical phonons. ρ_L is the material mass density. $\hbar\omega_O$ is the energy of optical phonons. Ξ is the deformation potential of acoustic phonons. $\hbar\omega_q$ is the energy of acoustic phonons. $\bar{e}_{av}$ is the average piezoelectric interaction constant. Note that $\varepsilon_s = K_s\varepsilon_0$. Usually, the dispersion relation of phonons (ie,ω -**q** relation) is assumed by using the Einstein approximation for optical phonons as $\omega_q = \omega_O$ and the Debye approximation for acoustic phonons as $\omega_q = v_s q$, where v_s is the sound speed of acoustic phonons.

If the effect of screening is considered, then the interaction matrices given in Equation (34) will be modified by a screening factor as[23]

$$\left|M_q^{\text{screen}}\right|^2 = |M_q|^2\left[\frac{\varepsilon_0}{\varepsilon_{\text{screen}}(q,\omega)}\right]^2 \quad (35)$$

where $\varepsilon_{\text{screen}}(q,\omega)$ can be calculated from the Lindhard formula for dynamic screening,

$$\varepsilon_{\text{screen}}(q,\omega) = \varepsilon_0\left[1-\frac{e^2}{\varepsilon_0 q^2 V}\sum_{\mathbf{k}}\frac{f_{\mathbf{k}+\mathbf{q}}-f_{\mathbf{k}}}{E_{\mathbf{k}+\mathbf{q}}-E_{\mathbf{k}}-\hbar(\omega+i\delta)}\right]. \quad (36)$$

In Equation (36), δ is collision-damping factor that is usually presumed to approach zero ($\delta \to 0$). It can be shown that under the static screening limit as $\omega \to 0$, the Lindhard formula of Equation (36) will yield the form of the Thomas-Fermi theory for static screening as

$$\varepsilon_{\text{screen}}(q,0) = \varepsilon_0\left(1+\frac{q_s^2}{q^2}\right). \quad (37)$$

Here, q_s is the static screening wave number which can be evaluated by

$$q_s^2 = \frac{e^2}{\varepsilon_0 K_s}\frac{\partial n}{\partial\mu}, \quad (38)$$

where n is the electron number density and μ is its chemical potential. Using the full form of the Lindhard formula of Equation (36) will inevitably involve the issue of the couple modes for the interaction between electrons and polar optical phonons. These couple modes comprise the plasmonic modes of electrons and the polar modes of optical phonons. They are strongly affected by each other and cannot be treated separately. The subject regarding the coupled modes is very complicated and is most certainly beyond the scope of this work. For simplicity, the Thomas-Fermi static screening of Equation (38) will be employed in the following discussion. Figure 4 shows the results of the static screening wave number q_s calculated by Equation (38). The results indicate that if the quasi-Fermi level is well below the conduction band edge (ie, low electron number density), the value of q_s is smaller than $10^5\,\text{cm}^{-1}$. On the other hand, if the quasi-Fermi level is well above the conduction band edge (ie, high electron number density), the value of q_s is about $3\times10^6\,\text{cm}^{-1}$ or so. As it will be shown in the following, nonequilibrium LO phonons resulting from the electron-polar optical phonon interaction mostly accumulate with their wave numbers between $10^5\,\text{cm}^{-1}$ and $10^7\,\text{cm}^{-1}$. The static screening will become very effective if its q_s is located at this range. In other words, the screening effects will become a prominent and crucial

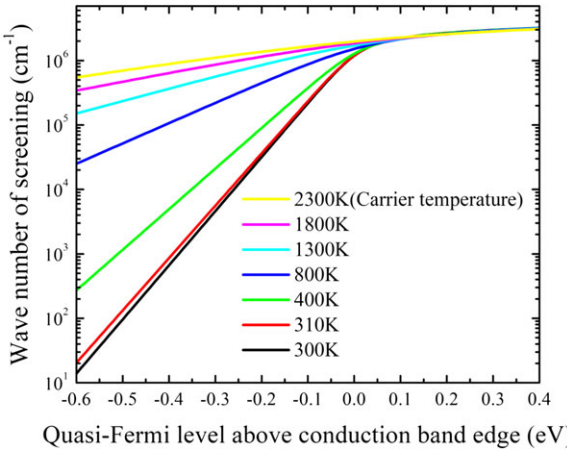

FIGURE 4 Wave number of the Thomas-Fermi static screening as a function of the quasi-Fermi level of conduction electrons at different carrier temperature [Colour figure can be viewed at wileyonlinelibrary.com]

factor for cases with high electron number density and a less concerning issue for cases with low electron number density. This fact will be verified in the following discussion.

For polar materials like III-V or II-VI compounds, carriers interact most strongly with the longitudinally polarized optical phonons (ie, LO phonons), as shown in the results of Figure 5. The scattering rate of polar LO phonons is at least 1 order of magnitude larger than other processes. In addition, optical phonons have a larger energy than acoustic phonons and thus provide a much more efficient channel for carriers to relax their energy. As a result, only the polar LO phonons will be considered for carrier energy relaxation processes in the following discussion.

An explicit formula for calculating Equation (32) can be derived without any simplification for the interaction of polar LO phonons as

$$\left(\frac{dN_{\mathbf{q}}}{dt}\right)_{c\to LO} = \frac{N_{\mathbf{q}}(T_c) - N_{\mathbf{q}}}{\tau_q^{c\text{-}LO}}. \tag{39}$$

Here,

$$N_{\mathbf{q}}(T) = \left[\exp\left(\frac{\hbar\omega_{\mathbf{q}}}{k_B T}\right) - 1\right]^{-1} \tag{40}$$

is the Bose-Einstein distribution function for phonons with energy $\hbar\omega_q$ at temperature T. The net emission time of LO phonons $\tau_q^{c\text{-}LO}$ in Equation (39) can be directly calculated from the following explicit formula as

$$\frac{1}{\tau_q^{c\text{-}LO}} = \frac{m_c^2 k_B T_c \left|M_q^{screen}\right|^2 V_c}{\pi\hbar^5 q} \ln\left[\frac{\exp(\eta_c - \varepsilon_{min} + \varepsilon_{LO}) + 1}{\exp(\eta_c - \varepsilon_{min}) + 1}\right], \tag{41}$$

where the dimensionless energy quantities are defined as $\eta_c = \mu_c/k_B T_c$, $\varepsilon_{LO} = \hbar\omega_{LO}/k_B T_c$, and $\varepsilon_{min} = \hbar^2 k_{min}^2/2m_c k_B T_c$ with $k_{min} = q/2 + m_c\hbar\omega_{LO}/\hbar^2 q$. Without considering nonequilibrium hot phonons, the mean phonon number $N_{\mathbf{q}}$ in Equation (39) will be given by the Bose-Einstein function of Equation (40) at a phonon temperature T_L, then Equation (39) will become

$$\left(\frac{dN_{\mathbf{q}}}{dt}\right)_{c\to LO} = \frac{N_{\mathbf{q}}(T_c) - N_{\mathbf{q}}(T_L)}{\tau_q^{c\text{-}LO}}. \tag{42}$$

In short, the intraband carrier energy relaxation via carrier-polar LO phonon interaction can be calculated explicitly by using Equations (33) to (42) without incorporating the effects of nonequilibrium hot phonons.

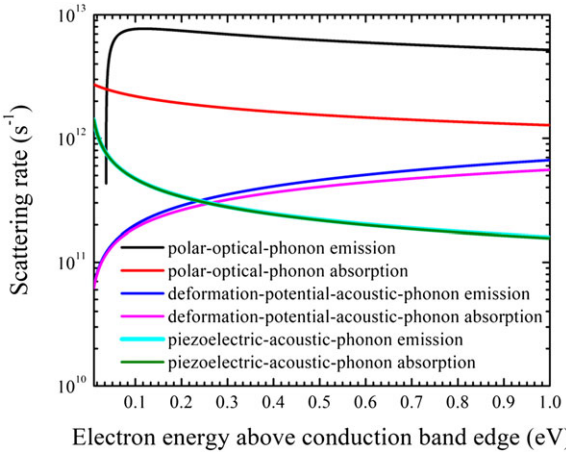

FIGURE 5 Electron scattering rates as a function of electron energy from the conduction band edge from different scattering processes of phonon emissions and absorptions: polar optical phonons, deformation potential acoustic phonons, and piezoelectric acoustic phonons. Note that the deformation potential optical phonons are prohibited for electrons at the Γ valley of the conduction band [Colour figure can be viewed at wileyonlinelibrary.com]

2.4 | Nonequilibrium hot phonons

Nonequilibrium hot optical phonons can be incurred by 2 factors: their negligible group velocity and their long decay times into acoustic phonons. The optical phonons emitted by carriers in intraband processes are in nature with small wave numbers and are thus located very near the zone center. The group velocity of optical phonons near the zone center is usually extremely small, and thus, they will not participate in the phonon heat transport. Once emitted by carriers, optical phonons will generally decay into acoustic phonons, which then propagate their energy away to diminish the accumulation of optical phonons and facilitate the overall carrier energy relaxation processes. If the decay rate of optical phonons into acoustic phonon is much slower than their net emission rate from carriers, with their negligible group velocity, optical phonons will accumulate at the spot of carrier emitting them and thus have a greater chance to be reabsorbed by carriers and impeding the overall carrier energy relaxation processes. As a result, it is essential to incorporate the decay process optical phonons into the carrier intraband energy relaxation processes. Consequently, the net emission rate of LO phonons can be calculated as

$$\frac{dN_{\mathbf{q}}}{dt} = \left(\frac{dN_{\mathbf{q}}}{dt}\right)_{c\to LO} + \left(\frac{dN_{\mathbf{q}}}{dt}\right)_{LO\to A_1+A_2}. \tag{43}$$

In Equation (43), the decay of an LO phonon into 2 acoustic phonons is a 3-phonon process which can be characterized by a lifetime τ_{LO}^0 near 0 K as[23]

$$\begin{aligned}\left(\frac{dN_{\mathbf{q}}}{dt}\right)_{LO\to A_1+A_2} &= -[N_{\mathbf{q}} - N_{\mathbf{q}}(T_L)]\frac{N_{\mathbf{q}_1}(T_L) + N_{\mathbf{q}_2}(T_L) + 1}{\tau_{LO}^0} \\ &= -\frac{N_{\mathbf{q}} - N_{\mathbf{q}}(T_L)}{\tau_{LO}}.\end{aligned} \tag{44}$$

In Equation (44), $N_{\mathbf{q}_1}(T_L)$ and $N_{\mathbf{q}_2}(T_L)$ are the equilibrium population numbers of acoustic phonon at wave vectors $\mathbf{q}_1$ and $\mathbf{q}_2$ emitted by an LO phonon with a wave vector $\mathbf{q} = \mathbf{q}_1 + \mathbf{q}_2$. The decay time (also named as lifetime) of LO phonons at lattice temperature T_L is then given by

$$\tau_{LO} = \frac{\tau_{LO}^0}{N_{\mathbf{q}_1}(T_L) + N_{\mathbf{q}_2}(T_L) + 1}. \tag{45}$$

Note that τ_{LO}^0 denotes the lifetime of LO phonons near 0 K, while τ_{LO} denotes the lifetime of LO phonons at T_L lattice temperature. For GaAs, a zone-centered LO phonon emitted by a carrier is likely to decay into a pair of acoustic phonons. It is interesting to mention that the issue regarding the decay routes of optical phonons is far more

complicated for some materials, such as GaN. They have been discussed in our previous work[24] and will not be discussed here for simplicity.

Substituting Equations (39) and (44) into Equation (43), the net mission rate of LO phonons can thus be calculated. At steady state, where $dN_{\mathbf{q}}/dt = 0$ in Equation (43), the nonequilibrium phonon population can be explicitly expressed as

$$N_{\mathbf{q}} = \frac{N_{\mathbf{q}}(T_c)/\tau_{\mathbf{q}}^{c\text{-}LO} + N_{\mathbf{q}}(T_L)/\tau_{LO}}{1/\tau_q^{c\text{-}LO} + 1/\tau_{LO}}. \quad (46)$$

In this theoretical model, the reason for calling LO phonons as nonequilibrium can be seen from Equation (46) in which the mean phonon number $N_{\mathbf{q}}$ at some wave vector $\mathbf{q}$ cannot be described by the equilibrium distribution of $N_{\mathbf{q}}(T_L)$ at T_L or $N_{\mathbf{q}}(T_c)$ at T_c. In other words, they are nonequilibrium phonons and their mean number cannot be described by the Bose-Einstein distribution function.

The formation of nonequilibrium LO phonons is strongly influenced from carrier temperature, carrier number density, and the effectiveness of screening, as shown in Figures 6 and 8, respectively. This can be further illustrated by examining the competition between the emission and decay rates of LO phonons, as shown in Figures 7 and 9, respectively. Apparently, if the emission rate of LO phonons $1/\tau_q^{c\text{-}LO}$ is much smaller than their decay rate $1/\tau_{LO}$, especially at low carrier number density or low carrier temperature, the formation nonequilibrium LO phonons will subside and their effects will become insignificant and negligible (Figure 8). Contrarily, if the emission rate of LO phonons is larger than their decay rate, especially at high carrier number density or high carrier temperature, the formation nonequilibrium LO phonons will be strongly enhanced and their effects will become significant and thus cannot be neglected.

Substituting Equation (46) into (39), the net emission rate of LO phonons at steady state can be calculated by

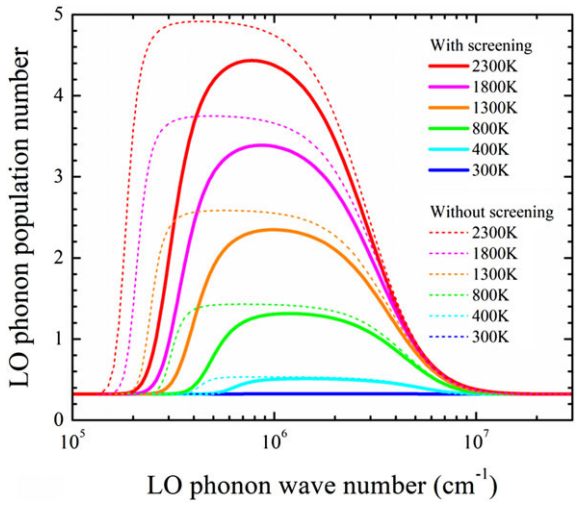

FIGURE 6 Longitudinal optical phonon statistically average population number as a function of phonon wave number at different electron temperatures with electron number density of 10^{18} cm^{-3} in GaAs. The correspondent dotted lines represent the calculated results without the effects of Thomas-Fermi static screening [Colour figure can be viewed at wileyonlinelibrary.com]

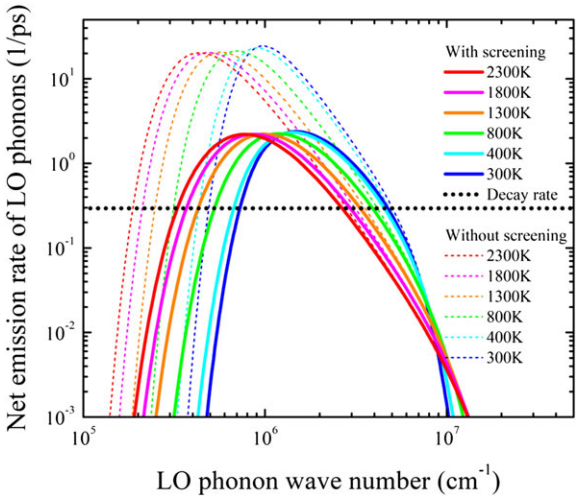

FIGURE 7 Net emission rates of longitudinal optical (LO) phonons as a function of phonon wave number at different electron temperatures with an electron number density of 10^{18} cm^{-3} in GaAs. The correspondent dotted lines represent the calculated results without effects of the Thomas-Fermi static screening. The black dotted line represents the decay rate of LO phonons [Colour figure can be viewed at wileyonlinelibrary.com]

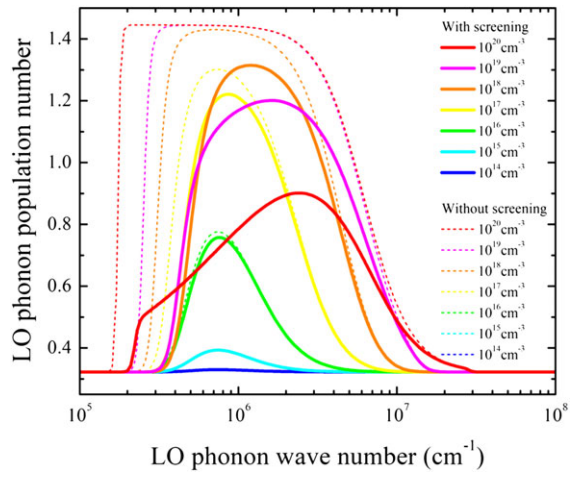

FIGURE 8 Longitudinal optical phonon statistically average population number as a function of phonon wave number with different electron density at electron temperature of 800 K in GaAs. The corresponding dotted lines represent the calculated results without effects of the Thomas-Fermi static screening [Colour figure can be viewed at wileyonlinelibrary.com]

$$\left(\frac{dN_{\mathbf{q}}}{dt}\right)_{c\text{-}LO} = \frac{N_{\mathbf{q}}(T_c) - N_{\mathbf{q}}(T_L)}{\tau_q^{c\text{-}LO} + \tau_{LO}}. \quad (47)$$

As a result, an explicit expression for calculating the intraband energy relaxation rate at steady state can consequently be obtained as

$$\left(\frac{du}{dt}\right)_{intra} = -\frac{1}{2\pi^2}\int_0^\infty dq\ q^2\,\hbar\omega_{LO}\frac{N_q(T_c) - N_q(T_L)}{\tau_q^{c\text{-}LO} + \tau_{LO}} \equiv -\frac{u(T_c) - u(T_L)}{\tau_E^{c\text{-}LO}}. \quad (48)$$

Here, the carrier energy relaxation time $\tau_E^{c\text{-}LO}$ is defined at a constant carrier density to characterize the time scale that carriers relax

their energy to LO phonons to equalize their temperature to lattice temperature.

Relaxation rates of electron energy density defined in Equation (48) as a function of electron number density with and without the effects of nonequilibrium hot LO phonons or the Thomas-Fermi static screening are calculated, as shown in Figure 10. It evidently indicates that the intraband electron energy relaxation without the effects of nonequilibrium hot LO phonons will be significantly overestimated by almost an order of magnitude at high carrier number density. This result illustrates the necessity of incorporating nonequilibrium optical phonons into the study of electron energy relaxation processes. The results also show that the effectiveness of static screening on electron energy relaxation rate becomes very substantial at large electron number density. This can be understood from the results of Figure 9. When electron density reaches 10^{20} cm^{-3}, the static screening becomes so effective, its effect alone will suppress net LO phonon emission rate to a value even smaller than the LO decay rate. However, in realistic cases, devices rarely operate with such a level of carrier number density. In addition, at such a large carrier density, the validity of static screening itself will become questionable.

For the purpose of comparison, the results of using the classical Boltzmann distribution function for carriers with a constant energy relaxation time of 0.1 ps (which roughly corresponds to the scattering time of LO phonon emission in Figure 5) are also shown in Figure 10. Although it agrees well with our results for low carrier number density (smaller than 10^{16} cm^{-3} here), it would be totally unrealistic and inappropriate by overestimating the electron intraband energy relaxation rates even to several orders of magnitude at high carrier number density. This clearly demonstrates that the method of using the classical Boltzmann distribution function for carriers with a single energy relaxation time is inadequate and unsuitable for studying carrier heating problems.

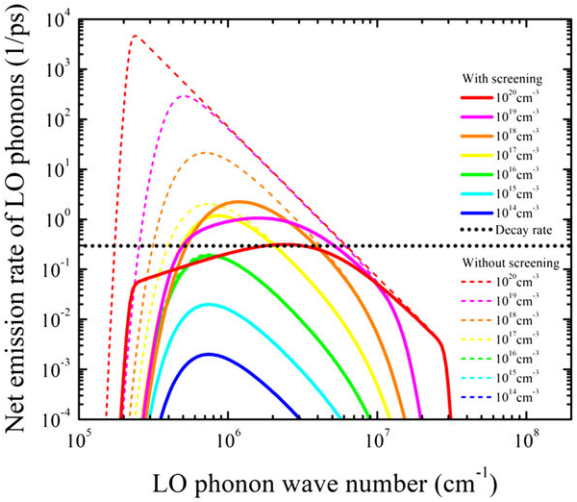

FIGURE 9 Net emission rates of longitudinal optical (LO) phonons as a function of phonon wave number with different electron number densities at electron temperature of 800 K in GaAs. The corresponding dotted lines represent the calculated results without effects of the Thomas-Fermi static screening. The black dotted line represents the decay rate of LO phonons [Colour figure can be viewed at wileyonlinelibrary.com]

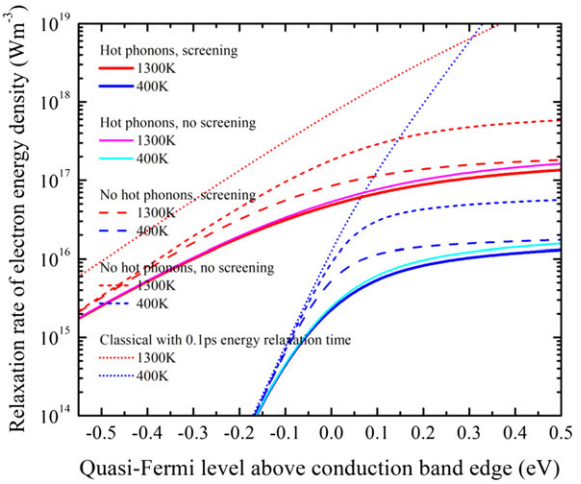

FIGURE 10 Relaxation rates of electron energy density as a function of the quasi-Fermi level of electrons in the conduction band at 400 and 1300 K carrier temperatures, respectively. The lattice temperature is 298.15 K. Comparisons are given for the results with or without the effects of nonequilibrium hot phonons or the Thomas-Fermi static screening [Colour figure can be viewed at wileyonlinelibrary.com]

It should be reminded here that the carrier energy relaxation time defined in Equation (48) is rather provisional. It is never a constant value, but in fact strongly dependent of carrier density, carrier temperature, and the effectiveness of screening, as shown in the calculated results in Figure 11. The results certainly confirm the inadequacy of the classical method or theoretical models' absence from hot-phonon effects in the study of carrier heating problems.

The typical values of the lifetime (ie, decay time) of optical phonons near 0 K lattice temperature are about 10 picoseconds from experimental measurements or theoretical estimations. However, only limited materials, such as GaAs, have their lifetimes of optical phonon being studied. Therefore, GaAs will be used as an example in the

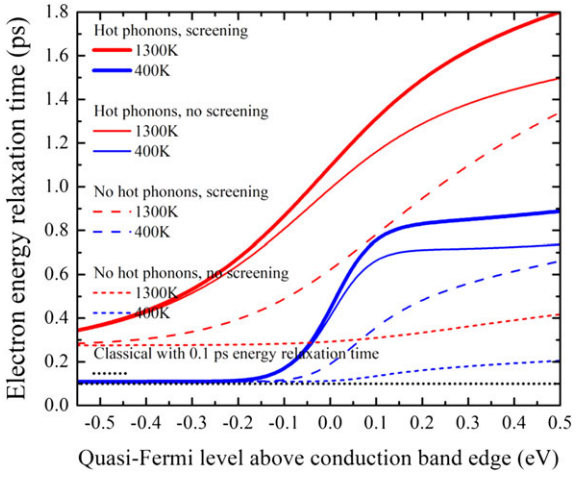

FIGURE 11 Electron energy relaxation time as a function of the quasi-Fermi level of electrons in the conduction band at 400 and 1300 K carrier temperatures, respectively. The lattice temperature is 298.15 K. Comparisons are given for the results with or without the effects of nonequilibrium hot phonons or the Thomas-Fermi static screening [Colour figure can be viewed at wileyonlinelibrary.com]

following calculations and discussion. Nevertheless, the theoretical model presented here should be general enough to apply for a wide range of carrier heating problems. Electron energy relaxation times as a function of LO phonon lifetime are also shown in Figure 12. As it can be expected that longer LO phonon lifetimes will certainly encourage the formation of nonequilibrium LO phonons and thus incur longer carrier energy relaxation time.

3 | RESULTS AND DISCUSSION

After introducing the theoretical model that comprises the rate equations for carrier number and energy densities and the formulas for calculating the radiative recombination current and power densities and the intraband energy relaxation rate of carrier-polar-LO-phonon interaction with the effects of nonequilibrium hot phonons and the Thomas-Fermi static screening, we will implement these rate equations and their associated formulas to simulate carrier-heating problems in bulk GaAs solar cells. It should be particularly reminded here that the theoretical model presented in this work does not distinguish the possibility of existing different temperatures for electrons in the conduction band and holes in the valence band by assuming the energy transfer between electrons and holes sufficient enough to maintain a common temperature.[25] However, due to their smaller density-of-state effective mass, electrons usually play a more active role in the problem of carrier heating than holes. Figure 13 shows the quasi-Fermi-level energy of electrons and holes under equal-injection conditions in GaAs as a function of carrier number density at different carrier temperatures. Apparently, quasi-Fermi-levels of electrons will increase more significantly than those of holes at larger carrier density or higher carrier temperature. As carrier density or temperature increases, electrons have a much greater chance of occupying higher energy states than holes and consequently have more efficient channels to emit phonons and relax their energy. As a result, only electron energy relaxation processes will be considered in this work. However, the theoretical model here can also be extended to accommodate the separate problems of hole heating, like in our previous work.[26]

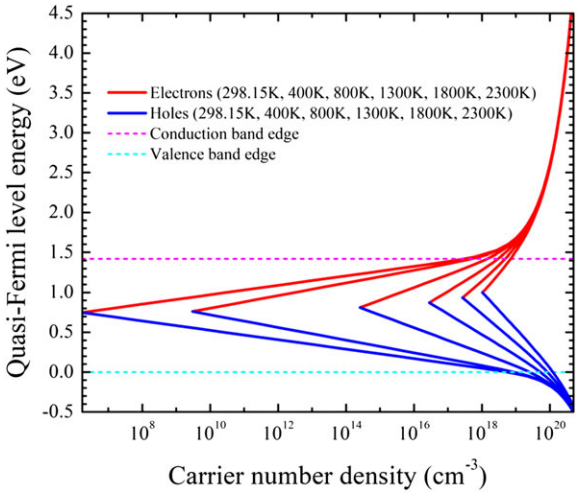

FIGURE 13 Quasi-Fermi levels of electrons and holes as a function of carrier density at different carrier temperature in GaAs [Colour figure can be viewed at wileyonlinelibrary.com]

To understand the numerical simulation of the carrier-heating problems from the rate equations of Equations (2) and (3), the carrier injection power density from the $J \cdot V$ and the intraband relaxation $L(du/dt)_{\text{intra}}$ in Equation (3) are calculated as a function of a device's voltage with different carrier temperatures and concentrator ratios for photovoltaic devices operating with concentrators, as shown in Figure 14, in which the current density J is calculated from Equation (2) without considering carrier heating from Equation (3). Evidently, for photovoltaic device operating near the short-circuit point, the energy

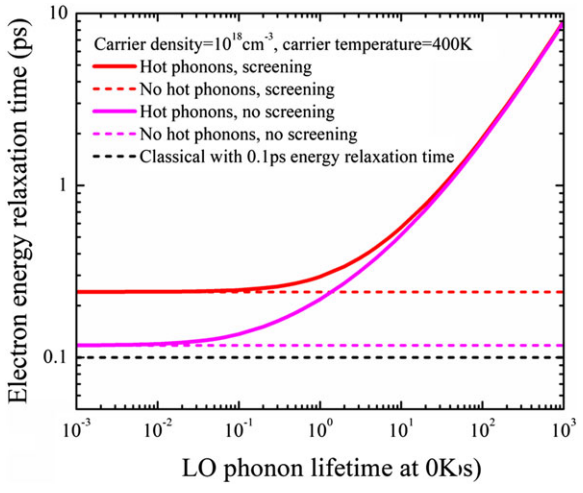

FIGURE 12 Electron energy relaxation time as a function of longitudinal optical (LO) phonon lifetime. The carrier density is 10^{18}cm^{-3}, and the carrier temperature is 400 K. The lattice temperature is 298.15 K. Comparisons are given for the results with or without the effects of nonequilibrium hot phonons or the Thomas-Fermi static screening. Note that the typical value for LO phonon lifetime at 0 K is about 10 ps [Colour figure can be viewed at wileyonlinelibrary.com]

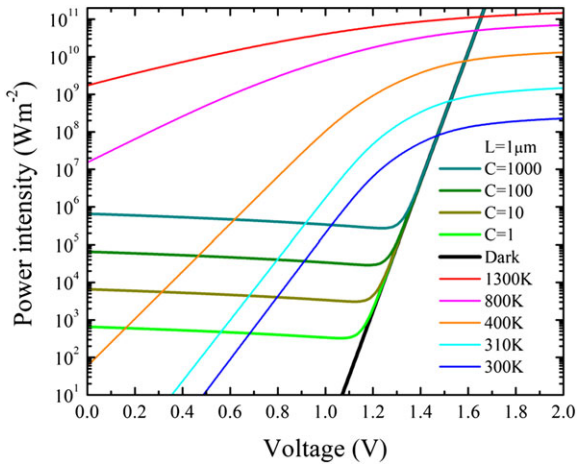

FIGURE 14 Power intensity from the $J \cdot V$ with different concentration ratios and the intraband relaxation $L(du/dt)_{\text{intra}}$ with different carrier temperatures in Equation (3) as a function of voltage, where $L = 1\,\mu\text{m}$. The current density J is calculated only from Equation (2) without carrier heating [Colour figure can be viewed at wileyonlinelibrary.com]

injected from the sunlight is several orders-of-magnitude more than the energy relaxed by carriers, unless the carrier temperature increases to several hundred degrees to balance the energy injection and relaxation. On the contrary, when the device's voltage approaches its open-circuit point, the energy relaxed by carriers becomes much larger than the energy injected from the sunlight, and thus, the carrier heating will eventually diminish. These conjectures will be confirmed in the following simulation results. In addition, when the device operates as a common diode with and applied voltage, the power generated from the dark current times the applied voltage will become extremely large if the applied voltage exceeds the band-gap energy (1.42 V for GaAs); it thus can be expected that the degree of carrier heating will become exceedingly significant. This speculation can also be verified from the simulation results here.

Apparently, the width of the active region L in Equation (3) is also a key parameter for the overall intraband energy relaxation in a device. In Figure 15, the injection rate of power intensity from the $J \cdot V$ and the intraband relaxation $L(du/dt)_{intra}$ in Equation (3) is a function of the applied voltage at 400 K carrier temperatures and 298.15 K lattice temperature with different width of the active region L. Here, the current density J is calculated only from Equation (2) without carrier heating. Devices with larger width of the active region will have a higher intraband power relaxation, and thus, their degree of carrier heating will be smaller. On the contrary, devices with smaller width of the active region will have a lower intraband power relaxation, and therefore, their degree of carrier heating will be much more severe. As a result, it can be presumably conjectured that solar cells with smaller active region, such as quantum wells and dots, will have a higher degree of carrier heating.

Figures 16 and 17 show the simulation results of carrier temperatures and the J-V relation, respectively, for GaAs material with L = 1 μm length of active region under different concentrator ratios. To demonstrate the applicability of the theoretical model, the range

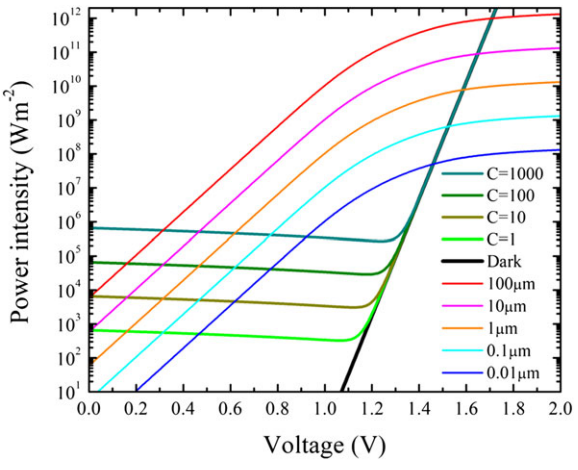

FIGURE 15 Injection rate of power intensity from the $J \cdot V$ with different concentration ratios and the intraband relaxation $L(du/dt)_{intra}$ with different width of the active region L in Equation (3) as a function of the applied voltage at 400 K carrier temperatures and 298.15 K lattice temperature. The current density J is calculated only from Equation (2) without carrier heating [Colour figure can be viewed at wileyonlinelibrary.com]

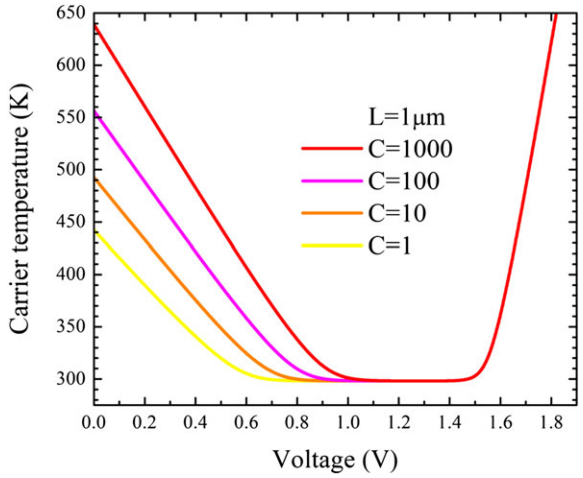

FIGURE 16 Carrier temperature as a function of device's voltage for different concentrator ratios with L = 1 μm [Colour figure can be viewed at wileyonlinelibrary.com]

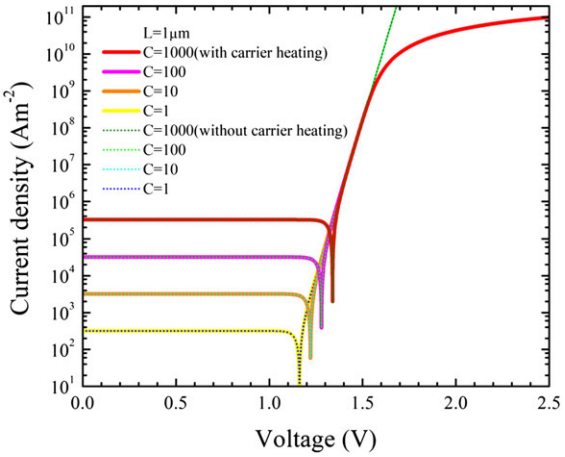

FIGURE 17 Current-voltage relation for different concentrator ratios with L = 1 μm. The corresponding dotted lines are the results without carrier heating. They are almost indistinguishable from the results with carrier heating for voltages smaller than 1.4 V. For devices operating as solar cells, the sign of their output current is minus here, and thus, the current density is set to be an absolute value [Colour figure can be viewed at wileyonlinelibrary.com]

of the voltage is simulated beyond the open-circuit voltage in which the photovoltaic device operates with an applied voltage like a common diode. Figure 18 demonstrates that carriers can be heated up to several hundred degree above the lattice temperature inside a solar cell even without a solar concentrator (ie, C = 1). However, as the device's voltage approaches the open-circuit point, the carrier energy relaxation becomes more efficient, and thus, the degree of carrier heating will eventually diminishes and completely vanish. As indicated in Equation (19), J_{sc} will be larger for semiconductors with smaller band-gap energies. On the contrary, V_{oc} will be larger (from a smaller J_0) for semiconductors with larger band-gap energies as indicated in Equations (17) and (20). As a result, it can be expected that photovoltaic devices with materials of smaller band-gap energies will have a higher degree of carrier heating and thus a larger carrier kinetic

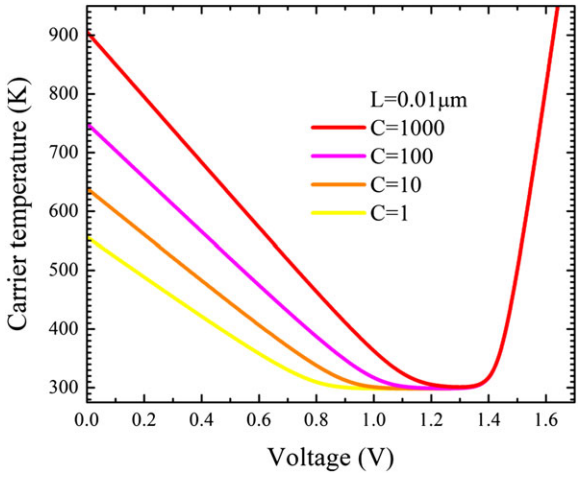

FIGURE 18 Carrier temperature as a function of device's voltage for different concentrator ratios with L = 0.01 μm [Colour figure can be viewed at wileyonlinelibrary.com]

energy. These suggest that photovoltaic devices with materials of smaller band-gap energies will have a better chance to be realized into hot-carrier solar cells in which the kinetic energy of hot carriers can be extracted as an additional output power.

If the device operates with an externally applied voltage, the carrier heating will become more severe again due to the extra power injected into the device by this external voltage source. The effects of carrier heating on the *J-V* relation are shown in Figure 17. When the device operates as a solar cell, carrier heating barely has any effect on it. Nevertheless, if the device operates with an extra applied voltage, the effects of carrier heating will saturate the output current with high applied voltage and consequently strongly deviate the *J-V* relation of an ideal from its exponential form. Simulation is also given to the case with 0.01-μm length of active region, as shown in Figures 18 and 19. For devices with smaller L, carrier heating will become more severe and its effects the *J-V* relation will become more prominent.

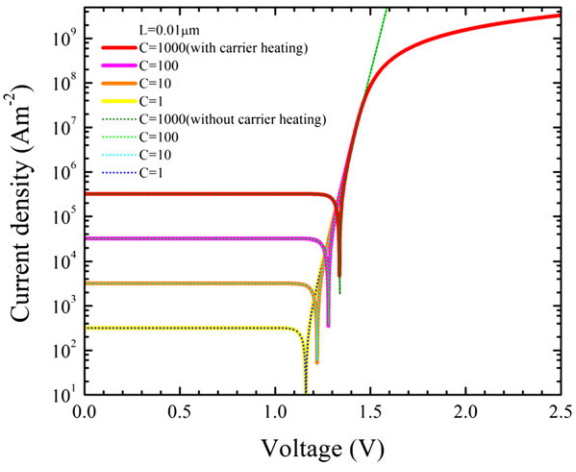

FIGURE 19 Current-voltage relation for different concentrator ratios with L = 0.01 μm. The corresponding dotted lines are the results without carrier heating. They are almost indistinguishable from the results with carrier heating for voltage smaller than 1.4 V. Here, current density is set to be an absolute value [Colour figure can be viewed at wileyonlinelibrary.com]

Simulations are also done for devices with different sizes of the active region under one-sun (C = 1) condition, as shown in Figures 20 and 21. As it can be expected, the degree of carrier heating will be smaller for devices with a larger width of the active region. On the contrary, devices with a smaller width of the active region will have a higher degree of carrier heating. As a result, these results certainly suggest that solar cells with a smaller active region, such as quantum wells and dots, will have a higher degree of carrier heating.

The simulation results demonstrate that incident sunlight indeed provides enough power onto the device to establish the condition of hot carriers when the device operates close its short-circuit condition. Figure 22 shows the simulation results of the carrier temperature as a function of the width of the active region with different concentration ratios under the short-circuit condition. For GaAs, carrier temperature ranges from 400 to 900 K at the short-circuit condition. The

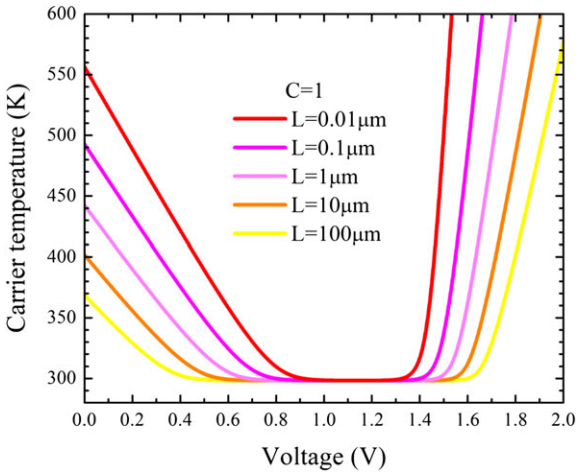

FIGURE 20 Carrier temperature as a function of device's voltage for different widths of the active region with C = 1 [Colour figure can be viewed at wileyonlinelibrary.com]

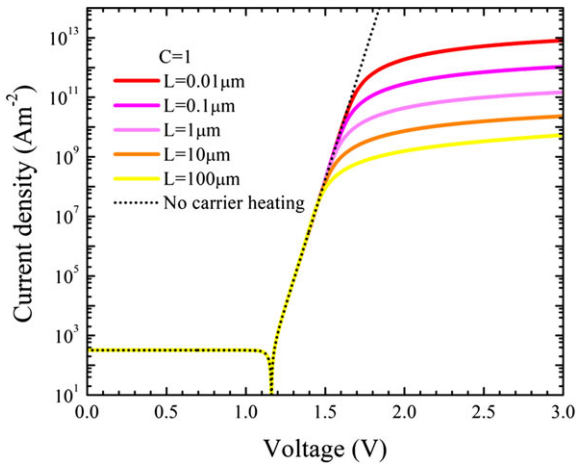

FIGURE 21 Current-voltage relation for different widths of the active region with C = 1. The black lines are the results without carrier heating. They are almost indistinguishable from the results with carrier heating for voltages smaller than 1.4 V. Here, current density is set to be an absolute value [Colour figure can be viewed at wileyonlinelibrary.com]

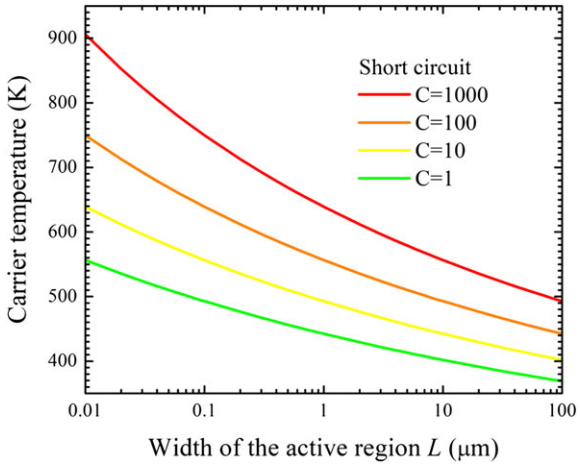

FIGURE 22 Carrier temperature as a function of the width of the active region at the short-circuit condition with different concentration ratios [Colour figure can be viewed at wileyonlinelibrary.com]

difference between carrier temperature T_c and lattice temperature T_{cell} is neither insignificant and nor negligible as assumed by conventional theory. In other words, the assumption of $T_c \simeq T_{cell}$ becomes questionable. However, as the output voltage increase, these hot carriers will relax their kinetic energy to phonons and eventually reach thermal equilibrium with phonons. As a result, they provide no contribution to the output power. This description can be further illustrated if carrier temperatures in Figure 22 are represented by the definition of the Carnot efficiency defined by Equation (25), as shown in Figure 23. Theoretically speaking, if the kinetic energy of hot carriers can be transformed into useful work, then this Carnot efficiency simply indicates the additional maximum achievable efficiency of thermodynamic limit. The possible ways of realizing such hot-carrier solar cells have been extensively studied and investigated[7-15]; and such a topic is certainly beyond the scope and capacity of this work.

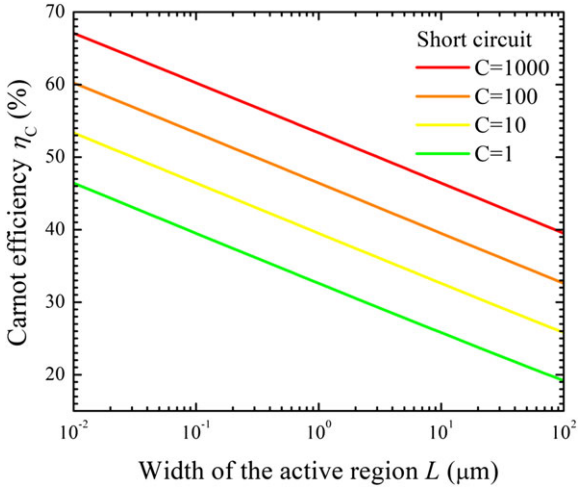

FIGURE 23 Carnot efficiency defined in Equation (25) as a function of the width of the active region at the short-circuit condition with different concentration ratios [Colour figure can be viewed at wileyonlinelibrary.com]

4 | CONCLUSION

A theoretical model and its rate equations of carrier number and energy densities have been proposed and presented for calculating carrier heating with effects of nonequilibrium hot phonons in semiconductor photovoltaic devices. The rate equation for carrier number density is identical to the SQ theoretical model, while the rate equation for carrier energy density includes the carrier interband energy relaxation via carrier radiative recombination and the carrier intraband energy relaxation via carrier via the interactions between carriers and polar LO phonons. The carrier intraband energy relaxation is calculated by incorporating the effects of nonequilibrium hot phonons and the Thomas-Fermi static screening. This model and its rate equations are employed for numerical simulations and calculations of the magnitude of carrier heating and its effects on the *J-V* relations of bulk GaAs solar cells under different concentration ratios and different widths of the active region. The simulation results demonstrate that carrier temperature in general heats up several hundred degrees under the short-circuit operating condition. These hot carriers eventually cool down to lattice temperature when the device approaches its open-circuit point even when operated under a high solar concentration.

The simulation and calculation results conclude that the degree of carrier heating is very noticeable near the short-circuit operating point and will diminish near the open-circuit operating point. Photovoltaic devices with smaller active regions or materials of smaller band-gap energies will have a higher degree of carrier heating and thus a larger carrier kinetic energy. In other words, these results suggest that photovoltaic devices formed with smaller active regions (such as with quantum wells or dots) or materials of smaller band-gap energies will have a better chance to be realized into hot-carrier solar cells in which the kinetic energy of hot carriers can be extracted as an additional output power.

ORCID

Chin-Yi Tsai http://orcid.org/0000-0002-4962-5912

REFERENCES

1. Shah J. *Hot Carriers in Semiconductor Nanostructures: Physics and Applications*. Academic Press, Inc.; 1992.
2. Leblebici Y, Kang SM. *Hot-Carrier Reliability of MOS VLSI Circuits*. Springer; 1993:15-53.
3. Fu J, Xu Q, Han G, et al. Hot carrier cooling mechanisms in halide perovskites. *Nat Commun*. 2017;8(1):1300.
4. Green MA, Bremner SP. Energy conversion approaches and materials for high-efficiency photovoltaics. *Nat Mater*. 2017;16(1):23-34.
5. Hirst LC, Walters RJ, Führer MF, Ekins-Daukes NJ. Experimental demonstration of hot-carrier photo-current in an InGaAs quantum well solar cell. *Appl Phys Lett*. 2014;104(23):231115.
6. Dimmock JAR, Day S, Kauer M, Smith K, Heffernan J. Demonstration of a hot-carrier photovoltaic cell. *Prog Photovoltaics Res Appl*. 2014;22(2):151-160.
7. Green MA. Third generation photovoltaics: ultra-high conversion efficiency at low cost. *Prog Photovoltaics Res Appl*. 2001;9(2):123-135.
8. Green MA. *Third Generation Photovoltaic: Advanced Solar Energy Conversion*. Springer; 2006:69-80.

9. Conibeer GJ, Jiang CW, König D, Shrestha S, Walsh ST, Green MA. Selective energy contacts for hot carrier solar cells. *Thin Solid Films*. 2008;516(20):6968-6973.
10. König D, Casalenuovo K, Takeda Y, et al. Hot carrier solar cells: principles, materials and design. *Physica E*. 2010;42(10):2862-2866.
11. Le Bris A, Guillemoles JF. Hot carrier solar cells: achievable efficiency accounting for heat losses in the absorber and through contacts. *Appl Phys Lett*. 2010;97(11):113506.
12. Feng Y, Aliberti P, Veettil BP, et al. Non-ideal energy selective contacts and their effect on the performance of a hot carrier solar cell with an indium nitride absorber. *Appl Phys Lett*. 2012;100(5):053502.
13. Conibeer G, Guillemoles JF, Yu F, Levard H. *Hot Carrier Solar Cells. Advanced Concepts in Photovoltaics*, ed. by Nozik AJ, Conibeer G, Beard MC, Royal Society of Chemistry; 2014. 379–424 pp.
14. Würfel P, Brown AS, Humphrey TE, Green MA. Particle conservation in the hot-carrier solar cell. *Prog Photovoltaics Res Appl*. 2005;13(4):277-285.
15. Patterson R, Kirkengen M, Puthen B, Veettil KD, Green MA, Conibeer G. Phonon lifetimes in model quantum dot superlattice systems with applications to the hot carrier solar cell. *Sol Energy Mater Sol Cells*. 2014;94:1931-1935.
16. Dupré O, Vaillon R, Green MA. *Thermal Behavior of Photovoltaic Devices: Physics and Engineering*. Springer; 2017:29-74.
17. Bernardi M, Vigil-Fowler D, Lischner J, Neaton JB, Louie SG. Ab initio study of hot carriers in the first picosecond after sunlight absorption in silicon. *Phys Rev Lett*. 2014;112(25):257402.
18. Neges M, Schwarzburg K, Willig F. Monte Carlo simulation of energy loss and collection of hot charge carriers, first step towards a more realistic hot-carrier solar energy converter. *Sol Energy Mater Sol Cells*. 2006;90(14):2107-2128.
19. Jacoboni C, Lugli P. *The Monte Carlo Method for Semiconductor Device Simulation*. Springer-Verlag; 1989.
20. Moglestue C. *Monte Carlo Simulation of Semiconductor Devices*. Springer; 1993.
21. Tsai CY. Theoretical study of the effects of carrier transport, capture, and escape processes on solar cells with embedded nanostructures. *J Nanomaterials*. 2014;972597.
22. Shockley W, Queisser HJ. Detailed balance limit of efficiency of p-n junction solar cells. *J Appl Phys*. 1961;32(3):510-519.
23. Ridley BK. *Quantum Processes in Semiconductors*. 3rd ed. 1993 Clarendon Press:349-360.
24. Tsai CY, Chen CH, Sung TL, Tsai CY, Rorison JM. Theoretical modeling of nonequilibrium optical phonons and electron energy relaxation in GaN. *J Appl Phys*. 1999;85(3):1475-1480.
25. Tsai CY, Shih FP, Chen CH, Wu TY, Sung TL, Tsai CY. Effects of electron-hole energy transfer on the nonlinear gain coefficients in the small-signal modulation response of semiconductor lasers. *Appl Phys Lett*. 1997;71(13):1747-1749.
26. Tsai CY, Chen CH, Sung TL, Tsai CY, Rorison JM. Theoretical modeling of the small-signal modulation response of carrier and lattice temperatures with the dynamics of nonequilibrium optical phonons in semiconductor lasers. *IEEE J Select Topics Quantum Electron*. 1999;5(3):596-605.
27. Reif F. *Fundamentals of Statistical and Thermal Physics*. McGraw-Hill; 1965:269-273.

How to cite this article: Tsai C-Y. Theoretical model and simulation of carrier heating with effects of nonequilibrium hot phonons in semiconductor photovoltaic devices. *Prog Photovolt Res Appl*. 2018;26:808–824. https://doi.org/10.1002/pip.3021

APPENDIX A

BLACK-BODY RADIATION

The derivation of the formulas of the black-body radiation will be outlined in this Appendix to serve the purposes of the definitions of related physical quantities and their associate notations used in this work.

The photons in a black-body are assumed to be at thermal equilibrium with temperature T. Consequently, their statistically average number $N_{\mathbf{q}}$ at wave vector $\mathbf{q}$ with energy $E_{\mathbf{q}}$ is given by the Bose-Einstein distribution function as

$$N_{\mathbf{q}} = \frac{1}{e^{E_{\mathbf{q}}/k_B T} - 1}. \tag{49}$$

The number density of photons is therefore calculated by

$$n = \frac{2}{V}\sum_{\mathbf{q}} N_{\mathbf{q}}. \tag{50}$$

$\sum_{\mathbf{q}}\cdots$ denotes the summation of all the possible mode of photons with wave vector $\mathbf{q}$ where the degeneracy factor 2 is resulted from the assumption that each mode with wave vector $\mathbf{q}$ can accommodate 2 possible polarization. Similarly, the energy density of photons can be calculated by

$$u = \frac{2}{V}\sum_{\mathbf{q}} E_{\mathbf{q}} N_{\mathbf{q}}. \tag{51}$$

The black-body radiation can be treated as the photons escape from a small hole from a cavity full of a photon gas at thermal equilibrium with temperature T. It has been shown that the number of particles that escapes from a small hole of a cavity of a particle gas is equal to the number of particles which strikes the area of the hole. Under such a circumstance, the particle flux density ϕ can be calculated from the mean velocity $\bar{v}$ and the number density n of the particles as[27]

$$\phi = \frac{1}{4} n \bar{v}. \tag{52}$$

As a result, the flux of photon number density (in unit of $m^{-2}\ s^{-1}$) can be calculated by

$$\phi = \frac{1}{4} c n = \frac{c}{4} \cdot \frac{2}{V}\sum_{\mathbf{q}} N_{\mathbf{q}} \tag{53}$$

where c is the speed of light in vacuum. Similarly, the light intensity (also known as irradiance) in unit of Wm^{-2} can be calculated by

$$I = \frac{1}{4} c u = \frac{c}{4} \cdot \frac{2}{V}\sum_{\mathbf{q}} E_{\mathbf{q}} N_{\mathbf{q}}. \tag{54}$$

By knowing the relationship between the energy $E_{\mathbf{q}}$ and the wave vector $\mathbf{q}$ of photons (known as the dispersion relation) at vacuum, $E_{\mathbf{q}} = \hbar c q$, where $\hbar = h/2\pi$ is the reduced Planck constant, the summation over the wave vectors $\sum_{\mathbf{q}}\cdots$ can be transformed into the integration of the energy $\int_0^\infty dE \cdots$ as

$$\frac{2}{V}\sum_{\mathbf{q}} = \frac{2}{(2\pi)^3}\int d^3\mathbf{q} = \int_0^\infty dq \frac{q^2}{\pi^2} = \int_0^\infty dE \frac{E^2}{\pi^2 c^3 \hbar^3} = \int_0^\infty dE \rho_{\text{mode}}(E), \tag{55}$$

where the density of modes is defined as

$$\rho_{\text{mode}}(E) = \frac{E^2}{\pi^2 c^3 \hbar^3} = \frac{8\pi E^2}{c^3 h^3}. \tag{56}$$

The number density of photons in Equation (50) can therefore be explicitly calculated by

$$n = \int_0^\infty dE \rho_{\text{mode}}(E) \frac{1}{e^{E/k_B T} - 1} = \int_0^\infty n(E) dE, \tag{57}$$

where the definition of the spectral photon number density $n(E)$ is given. Similarly, the formulas for calculating the spectral photon energy density $u(E)$ from Equation (51), the spectral flux of photon number density $\phi(E)$ from Equation (53), and the spectral irradiance $I(E)$ from Equation (54) are listed in the following:

$$n(E) = \frac{8\pi E^2}{h^3 c^3} \frac{1}{e^{E/k_B T} - 1}, \tag{58}$$

$$u(E) = E n(E) = \frac{8\pi E^3}{h^3 c^3} \frac{1}{e^{E/k_B T} - 1}, \tag{59}$$

$$\phi(E) = \frac{1}{4} c n(E) = \frac{2\pi E^2}{h^3 c^2} \frac{1}{e^{E/k_B T} - 1}, \tag{60}$$

$$I(E) = E\phi(E) = \frac{1}{4} c u(E) = \frac{2\pi E^3}{h^3 c^2} \frac{1}{e^{E/k_B T} - 1}. \tag{61}$$

It is a common practice to express the above spectral light intensity by per unit wavelength, eg, $I(\lambda)$, rather than per unit photon energy, $I(E)$, where $I = \int_0^\infty I(\lambda) d\lambda = \int_0^\infty I(E) dE$ is ensued. For example, the standard solar spectral irradiance data ASTM-173-03 are given by per unit wavelength in unit of nanometers. By using the relation between energy E and wavelength λ, $E = hc/\lambda$, the relation between $I(\lambda)$ and $I(E)$ is given as $I(\lambda) = I(E)hc/\lambda^2$. The spectral physical quantities per unit wavelength are listed in the following:

$$n(\lambda) = \frac{8\pi}{\lambda^4} \frac{1}{e^{hc/\lambda k_B T} - 1}, \tag{62}$$

$$u(\lambda) = \frac{8\pi hc}{\lambda^5} \frac{1}{e^{hc/\lambda k_B T} - 1}, \tag{63}$$

$$\phi(\lambda) = \frac{2\pi c}{\lambda^4} \frac{1}{e^{hc/\lambda k_B T} - 1}, \tag{64}$$

$$I(\lambda) = \frac{2\pi hc^2}{\lambda^5} \frac{1}{e^{hc/\lambda k_B T} - 1}. \tag{65}$$

The above expressions for the black-body radiation are assumed to be observed at the proximity of an infinite plane of the heat source, which is certainly untrue for the solar radiation observed at the Earth. In the terminologies of radiometry and photometry, it is a general practice to distinguish between the physical quantities of the irradiance I (in unit of Wm^{-2}) and the radiance L (in unit of $Wm^{-2}\ sr^{-1}$). The irradiance I characterizes the overall radiation intensity received by an observer, while the radiance L characterizes the radiation intensity emitted from a point source. For radiation observed at the proximity of an infinite plane of a heat source, $I = \pi L$.

For solar radiation, the geometric factor associated with a finite-size black-body heat source needs to be taken into consideration, in which the photon flux density per unit energy per unit solid angle (or per steradian in SI unit), $\phi(E, \Omega)$, will be defined as

$$\phi = \iint \phi(E, \Omega) dE d\Omega. \tag{66}$$

The factor π in the Equation (60) will be replaced by a geometrical factor as

$$\phi(E, \Omega) = F_b(\Omega) \frac{2E^2}{h^3 c^2} \frac{1}{e^{E/k_B T} - 1}, \tag{67}$$

where $F_b(\Omega)$ denotes the geometrical factor. $F_b(\Omega) = \cos\theta$ in the spherical coordinate system at the observer end. The geometrical factor for observing at the Sun's proximity will be

$$\int_{\text{hemisphere}} F_b(\Omega) d\Omega = \int_0^{2\pi} d\phi \int_0^{\pi/2} d\theta \cos\theta \sin\theta = \pi. \tag{68}$$

The geometrical factor for observing the Sun from the Earth will become

$$F_{\text{sun}} = \pi \sin^2\left(\frac{\theta_{\text{sun}}}{2}\right) = \pi \cdot \left(\frac{r_{\text{sun}}}{d_{\text{sun-earth}}}\right)^2, \tag{69}$$

where $\theta_{\text{sun}} \approx 0.533^o$ is the angular diameter of the Sun which is related to its radius $r_{\text{sun}} = 6.96 \times 10^5$ km and its average distance from the Earth $d_{\text{sun - earth}} \approx 1.5 \times 10^8$ km as

$$\tan\frac{\theta_{\text{sun}}}{2} \approx \sin\frac{\theta_{\text{sun}}}{2} = \frac{r_{\text{sun}}}{d_{\text{sun-earth}}}, \tag{70}$$

where the approximate form is used for a spherical object. As a result, the theoretical value for the spectral AM0 black-body solar radiation with a characteristic photosphere temperature T_{sun} will become

$$\phi_{\text{AM0}}(E) = \frac{2\pi E^2}{h^3 c^2} \frac{1}{e^{E/k_B T_{\text{sun}}} - 1} \left(\frac{r_{\text{sun}}}{d_{\text{sun-earth}}}\right)^2. \tag{71}$$

Equation (71) has been used to fit the AM0 spectral solar irradiance ASTM-173-03 data with $T_{\text{sun}} = 5800$K, as shown in the Figure 1.

APPENDIX B

PRINCIPLE OF DETAILED BALANCE

In this appendix, it will be demonstrated that the relations between the spectral photon number density flux emitted from carriers $\phi_c(E)$ and absorbed from incident black-body ambient radiation $\phi_{\text{amb}}(E)$ given by the Equation (14) and (24) can be obtained from the principle

of detailed balance. The principle of detailed balance states that each physical process should be equilibrated by its reverse process when the system reaches its steady state. It is one of the fundamental principles in statistical mechanics and therefore should be applicable to the problem in this work.

The statistically average number of electrons in the **k**-state of the conduction band with energy E_{ck} at thermal equilibrium is given by the Fermi-Dirac distribution function as

$$f_{ck} = \left[\exp\left(\frac{E_{ck} - E_{Fc}}{k_B T_c}\right) + 1\right]^{-1}, \tag{72}$$

where E_{Fc} denotes the electrochemical potential (also named as quasi-Fermi level) energy of electrons in the conduction band. E_{ck} represents the energy-momentum (E-**k**) relation of the conduction band. Note that the carrier distribution function is characterized by the carrier temperature T_c in Equation (72). Similarly, the average number of electrons in the **k**-state of the valence band with energy E_{vk} is given by

$$f_{vk} = \left[\exp\left(\frac{E_{vk} - E_{Fv}}{k_B T_c}\right) + 1\right]^{-1}, \tag{73}$$

where E_{Fv} denotes the electrochemical potential energy of electrons in the valence band. E_{vk} represents the energy-momentum (E-**k**) relation of the valence band.

The interaction matrix between electrons and photons comprises 2 parts as

$$|\langle \cdots | H_{int} | \cdots \rangle|^2 = |M_{\mathbf{q}}|^2 (N_{\mathbf{q}} + 1) + |M_{\mathbf{q}}|^2 N_{\mathbf{q}}, \tag{74}$$

Here, H_{int} denotes the electron-photon interaction Hamiltonian. $|M_{\mathbf{q}}|$ represents the electron-photon interaction matrices. In Equation (74), the term with $N_{\mathbf{q}}$ + 1 denotes the emission process which contains the stimulated emission and the spontaneous emission processes, while the term with $N_{\mathbf{q}}$ denotes the absorption process. The average carrier number f_{ck} reduced by the photon emission process can thus be calculated by

$$\left(\frac{df_{ck}}{dt}\right)_{emission} = -\frac{2\pi}{\hbar}|M_{\mathbf{q}}|^2 (N_{\mathbf{q}} + 1) f_{ck}(1 - f_{vk}) \delta(E_{ck} - E_{vk} - E_{\mathbf{q}}). \tag{75}$$

Here, $\delta(E)$ is the Dirac delta function that characterizes the conservation of energy. Similarly, the average carrier number f_{ck} increased from the photon absorption process can be calculated by

$$\left(\frac{df_{ck}}{dt}\right)_{absoption} = \frac{2\pi}{\hbar}|M_{\mathbf{q}}|^2 N_{\mathbf{q}}(1 - f_{ck}) f_{vk} \delta(E_{ck} - E_{vk} - E_{\mathbf{q}}). \tag{76}$$

As a result, the net rate for the change rate of f_{ck} is given by

$$\begin{aligned} \frac{df_{ck}}{dt} &= \left(\frac{df_{ck}}{dt}\right)_{absoption} + \left(\frac{df_{ck}}{dt}\right)_{emission} \\ &= \frac{2\pi}{\hbar}|M_{\mathbf{q}}|^2 [N_{\mathbf{q}}(1 - f_{ck}) f_{vk} - (N_{\mathbf{q}} + 1) f_{ck}(1 - f_{vk})] \delta(E_{ck} - E_{vk} - E_{\mathbf{q}}). \end{aligned} \tag{77}$$

From the principle of detailed balance, $df_{ck}/dt = 0$ is assumed at steady state. Consequently,

$$N_{\mathbf{q}}(1 - f_{ck}) f_{vk} - (N_{\mathbf{q}} + 1) f_{ck}(1 - f_{vk}) = 0. \tag{78}$$

The photon number can thus be calculated from Equation (78) as

$$\begin{aligned} N_{\mathbf{q}} &= \frac{f_{ck}(1 - f_{vk})}{f_{vk} - f_{ck}} = \left[\exp\left(\frac{E_{ck} - E_{Fc} - E_{vk} + E_{Fv}}{k_B T_c}\right) - 1\right]^{-1} \\ &= \left\{\exp\left[\frac{E_{\mathbf{q}} - (E_{Fc} - E_{Fv})}{k_B T_c}\right] - 1\right\}^{-1} = \left[\exp\left(\frac{E_{\mathbf{q}} - qV}{k_B T_c}\right) - 1\right]^{-1}. \end{aligned} \tag{79}$$

Here,

$$V = (E_{Fc} - E_{Fv})/q \tag{80}$$

is defined as the separation of the electrochemical (ie, the quasi-Fermi levels) potentials of electrons and holes which is equal to the device voltage in the SQ theory.

In this problem, the photons that interact with the carriers in the cell are denoted as $N_{\mathbf{q}}^c$ in the following discussion (ie,$N_{\mathbf{q}} = N_{\mathbf{q}}^c$). Note that Equation (79) is always valid as long as the system operates at steady state, even if the system is not at thermal equilibrium with the ambient environment. However, if the device is at thermal equilibrium with the ambient environment with $T_c = T_{amb}$ and $V = 0$, Equation (79) will become

$$N_{\mathbf{q},V=0}^c = \left[\exp\left(\frac{E_{\mathbf{q}}}{k_B T_{amb}}\right) - 1\right]^{-1} \equiv N_{\mathbf{q}}^{amb}, \tag{81}$$

where $N_{\mathbf{q}}^{amb}$ denotes as the Bose-Einstein function of ambient photons at ambient temperature T_{amb}. When a conventional solar cell operates at steady-state at a output voltage V without hot-carrier effects, ie, $T_c = T_{amb} = T$, Equation (79) will yield the following result:

$$N_{\mathbf{q}}^c(T, V) = \left[\exp\left(\frac{E_{\mathbf{q}} - qV}{k_B T}\right) - 1\right]^{-1} \neq N_{\mathbf{q}}^{amb} \tag{82}$$

If the conditions of $E_{\mathbf{q}} \gg k_B T$ and $(E_{\mathbf{q}} - qV) \gg k_B T$ are satisfied, Equations (81) and (82) can be approximately expressed as

$$N_{\mathbf{q}}^{amb} \approx \exp\left(-\frac{E_{\mathbf{q}}}{k_B T}\right), \tag{83}$$

and also

$$N_{\mathbf{q}}^c(T, V) \approx \exp\left(-\frac{E_{\mathbf{q}} - qV}{k_B T}\right) = N_{\mathbf{q}}^{amb}\left(\frac{qV}{k_B T}\right). \tag{84}$$

From the definition in Equation (53), the spectral photon flux densities $\phi_{amb}(E)$ and $\phi_c(E)$ can be calculated from $N_{\mathbf{q}}^{amb}$ and $N_{\mathbf{q}}^c$ by doing the summation of all possible modes of $\sum_{\mathbf{q}} \cdots$. As a result,

$$\phi_c(E) = \phi_{amb}(E) \exp\left(\frac{qV}{k_B T}\right), \tag{85}$$

which yields Equation (14).

If the effects of hot carriers are considered when $T_c \neq T_{amb}$, then the $N_{\mathbf{q}}^c$ in Equation (82) can be expressed as

$$\begin{aligned} N_{\mathbf{q}}^c &\approx \exp\left(-\frac{E_{\mathbf{q}} - qV}{k_B T_c}\right) \\ &= N_{\mathbf{q}}^{amb} \exp\left[\frac{E_{\mathbf{q}}}{k_B T_{amb}}\left(1 - \frac{T_{amb}}{T_c}\right)\right] \exp\left(\frac{qV}{k_B T_{amb}} \cdot \frac{T_{amb}}{T_c}\right) \end{aligned} \tag{86}$$

where the term of $1 - T_{amb}/T_c$ is defines as the Carnot's efficiency,

$$\eta_C \equiv 1 - \frac{T_{amb}}{T_c}, \tag{87}$$

Consequently, Equation (86) can be rewritten as

$$N_{\mathbf{q}}^{c} = N_{\mathbf{q}}^{amb} \exp\left(\frac{\eta_C E_{\mathbf{q}}}{k_B T_{amb}}\right) \exp\left[\frac{(1-\eta_C) qV}{k_B T_{amb}}\right] \tag{88}$$

From the definition in Equation (53), the spectral flux of the photon number density $\phi_c(E)$ can be calculated from $N_{\mathbf{q}}^{c}$ in Equation (88) by doing the summation of all possible modes of $\sum_{\mathbf{q}} \cdots$, and the result is

$$\phi_c(E) = \phi_{amb}(E) \exp\left(\frac{\eta_C E}{k_B T_{amb}}\right) \exp\left[\frac{(1-\eta_C) qV}{k_B T_{amb}}\right], \tag{89}$$

which yields Equation (24). The expression of Equation (24) is a general result from the principle of detailed balance with only the assumption of photons emitted by carriers having energies much larger than the thermal energy (ie, $E_{\mathbf{q}} \gg k_B T$) and also the assumption of carriers participating in this photon emission mostly locating at the energy states much higher than its quasi-Fermi level energy (ie, $(E_{\mathbf{q}} - qV) \gg k_B T$). These 2 approximations are generally appropriate under most circumstances. Otherwise, the full form of Equation (79) needs to be employed, and the results will not be as straightforward to interpret.